Pergamon

Available online at www.sciencedirect.com
SCIENCE DIRECT®

Cement and Concrete Research 33 (2003) 1375–1383

CEMENT AND CONCRETE RESEARCH

Durability of traditional plasters with respect to blast furnace slag-based plaster

T. Cerulli, C. Pistolesi, C. Maltese*, D. Salvioni

Mapei SpA, Via Cafiero, 22, Milan 20158, Italy

Received 23 May 2002; accepted 18 February 2003

Abstract

Blast furnace slag is a residue of steel production. It is a latent hydraulic binder and is normally used to improve the durability of concrete and mortars. Slag could be also used as rendering mortar for masonry and old buildings. Today, cement and hydraulic lime are the most popular hydraulic binders used to make plasters. They are characterised by a low durability when exposed to the action of chemical and physical agents. The aim of this study was to provide a comparison between the physical–mechanical properties of some renders made with ordinary Portland cement, hydraulic lime, or slag. Furthermore, an investigation was carried out to analyse mortar resistance to several aggressive conditions like acid attack, freezing and thawing cycles, abrasion, sulphate aggression, cycles in ultraviolet screening device, and salt diffusion. The specimens, after chemical attack, have been characterised from the chemical–physical [specific surface according to the BET (Brunauer–Emmet–Teller) method], crystal–chemical (X-ray diffraction, XRD), and morphological (scanning electron microscopy, SEM) points of view.

Keywords: Acid attack; Durability; Plasters; Renders; Slag; Sulphate attack

1. Introduction

Since ancient times, rendering mortars have been used to protect masonry and monuments [1,2]. Several aspects of the durability of such materials were studied [2–4] and rules were developed to consider a mortar suitable for masonry and old buildings repair (WTA Austrian norms; prEN998-1). Today, the market is oriented toward the use of Portland cement or hydraulic lime-based plasters. Usually, an air-entraining admixture is utilised. This chemical causes air bubbles formation, improving mortar workability due to air insertion. Furthermore, such porosity increases the water vapour permeability of the plaster, reducing the degradation problems related to the presence of moisture in the masonry (e.g., freezing and thawing cycles, chemical damaging reactions) [5,6]. The use of blast furnace slag as a hydraulic binder for plasters could be very useful for two main reasons: (1) to get rendering mortars more similar to the ancient ones (latent hydraulic binders were commonly used in the past [7]), and (2) to increase mortar durability [8,9]. Blast furnace slag is a residue of steel manufacture and it could be an economic, energy-saving, and ecological material for the preparation of durable rendering mortars.

2. Scope

A study was carried out in order to analyse several types of plasters from the chemical, morphological, mechanical, and durability points of view. Acid attack, efflorescence simulation by salt diffusion, freezing and thawing cycles, Taber abrasion, sulphate aggression, and weathering were detected to evaluate mortar durability. Compressive strength, adhesion on brick, water absorption, specific gravity, total porosity, and water vapour permeability were also determined. Acid and sulphate attacks were studied by X-ray diffraction (XRD), thermogravimetric differential scanning calorimetry (TG-DSC), energy dispersive spectroscopy

* Corresponding author.
E-mail address: s-laboratorio@mapei-it (C. Maltese).

0008-8846/03/$ – see front matter © 2003 Elsevier Science Ltd. All rights reserved.
doi:10.1016/S0008-8846(03)00072-3

Table 1
Mortar mixture

Components	A	B	C	D	Characteristics
Blast furnace slag	28.00	–	–	–	Particle diameter = 22 μm determined by laser granulometry; Al_2O_3 = 17; MgO = 11; SiO_2 = 42; CaO = 29; SO_3 = 0.02
CEM I 52.5 (according to ENV 196/1)	–	62.0	15.80	–	Al_2O_3 = 4.6; CaO = 63.8; MgO = 2.05; SO_3 = 3.3; SiO_2 = 25.0
Normalized silica sand	69.95	10.95	–	50.00	0–2.5 mm
Air-entraining agent	0.05	0.05	0.05	–	–
Lightweight silica aggregate	–	13.00	–	–	0–2.5 mm
Hydrated lime	2.00	6.00	–	10.00	–
Calcium carbonate	–	8.00	84.20	25.00	0–2.5 mm
Hydraulic lime	–	–	–	15.00	CaO = 47; Al_2O_3 = 3.3; Fe_2O_3 = 2.4; SO_3 = 0.9; SiO_2 = 41.2
Water (% on the formulation)	15	67	22	17	–

(EDS), scanning electron microscopy (EDS), and specific surface area measurements by Brunauer–Emmet–Teller (BET) method.

3. Experimental

The mortar composition is reported in Table 1. The water amount was chosen to have a flow (determined according to UNI 7044) of about 90%. Such value allows to have an acceptable workability. The physical properties [specific gravity, air content (DIN 18555, Part 2), and flow] are shown in Table 2. After mixing (ENV 196/1), the plasters were used according to the foreseen experimental tests. All the samples were cured at 23 °C and 50% relative humidity (RH).

3.1. Physical–mechanical tests

The following physical mechanical tests were carried out after 28 days of curing according to the mentioned norms using prismatic specimens of size 40 × 40 × 160 mm, where otherwise specified:

Compressive strengths (ENV 196/1);
Adhesion on the prewetted surface of a brick having dimensions 400 × 200 × 40 mm (by pullout test) and cracks formation;
Unit weight of hardened samples (DIN 1060, Part 3);
Total porosity (by unit weight determination [5]);
Water absorption (UNI 7699); and
Water vapour permeability test (cylindrical specimens having dimensions 100 × 10 mm, DIN 52615 μ).

The results are shown in Table 2.

Table 2
Physical mechanical properties of fresh and hardened mortars

	A	B	C	D
Flow (% UNI 7044)	90	92	95	94
Air content (% DIN 18555, Part 2)	20	25	35	5
Unit weight (kg/m^3, by picnometer)	1850	950	1300	2070
Compressive strength	4.5	1.6	1.5	0.9
(7 and 28 days MPa)	5	2.5	1.9	1.3
Adhesion (MPa 28 days)/cracks	0.5/No	∅/No	∅/No	∅/No
Total porosity (%)	34	55	42	27
Water vapour permeability (μm)	21	9	8	14
Unit weight (after 28 of curing; kg/m^3)	1700	660	1140	1790
Water absorption (%)	14	32	17	13

Table 3
Acid resistance of rendering mortars

Sample	Residual strength (%)
A	86
B	81
C	0 (completely degraded)
D	50

3.2. Durability tests

3.2.1. Sulphuric acid attack

The test was used to evaluate sulphuric acid resistance. The specimens (40 × 40 × 80 mm) were cured for 28 days. Some of them were immersed into water (reference samples) and the others were dipped in sulphuric acid at pH = 0 (the test procedure is deeply explained elsewhere [10]). After 14 days, the residual mechanical resistance of the corroded samples with respect to the references (kept in water) was measured. The results are indicated in Table 3 (each value is an average of four measurements).

3.2.2. Efflorescence resistance test

Such a test was developed to simulate the rising and crystallisation of soluble salts in plasters applied on old masonry saturated by salts. This effect is particularly damaging for building materials [11]. Tuff bricks (100 × 200 ×

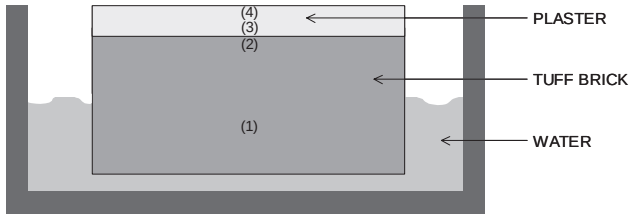

Fig. 1. Scheme of the efflorescence resistance test (Section 3.2.2).

Table 4
Efflorescence resistance

Cycles in the salty solution					
System	Extraction area	Conductivity after 24 h (ms/cm, σ24 h)	Conductivity after 28 days (ms/cm, σ28 days)	Conductivity increase (σ28 days − σ24 h)	Material recovered on the surface after cycles (g)
A	Tuff at medium height	10.6	14.7	4.1	1
	Tuff under plaster	10.2	13.8	3.6	
	Inferior part of the plaster	7.6	12.1	4.5	
	Superior part of the plaster	4.6	9	4.4	
B	Tuff at medium height	10.4	16.3	5.9	16
	Tuff under plaster	10.2	15.4	5.2	
	Inferior part of the plaster	10	26.6	16.6	
	Superior part of the plaster	9.3	29.6	20.3	
C	Tuff at medium height	11	17	6	6
	Tuff under plaster	10.7	15	4.3	
	Inferior part of the plaster	10	16.4	6.4	
	Superior part of the plaster	9.2	21.1	11.9	
D	Tuff at medium height	10.3	17	6.7	5
	Tuff under plaster	10.1	16.8	6.7	
	Inferior part of the plaster	9.6	18.2	8.6	
	Superior part of the plaster	8.9	20.1	11.2	

300 mm) were immersed for 3 days into a saturated solution of sodium chloride. Plaster was then applied on a brick surface. The system (brick + plaster) was subsequently subjected to the following cycle:

1. Dipped (at half brick height; Fig. 1) for 24 h in a saturated sodium chloride solution; and
2. Dried for 48 h at 23 °C and 50% RH.

The mentioned procedure was repeated for 28 days and the resulting powder, formed on the render surface (salt and degraded mortar), was weighed. After the first cycle and after 28 days, one brick was broken in the middle and some specimens were collected (two samples for each zone):

1. In the middle of tuff brick;
2. In the region of tuff brick close to the plaster;
3. In the lower part of the plaster (close to tuff brick); and
4. In the superficial part of the plaster.

Table 5
Freezing and thawing cycles

	A	B	C	D
Weight loss after 1 month (%)	∅	7	0	Destroyed
Weight loss after 2 months (%)	0.9	9	5	–

Table 6
Taber abrasion test

Sample	Weight loss (%)
A	21
B	11
C	The test specimens were destroyed after 10 rotations
D	The test specimens were destroyed after four rotations

These specimens were ground and dispersed in distilled water (1:4 ratio), and specific conductivity was measured. The results are reported in Table 4.

3.2.3. Freezing and thawing cycles

Freezing and thawing cycles were carried out on plaster specimens (after 28 days of curing) having dimensions of 100 × 100 × 100 mm, according to the following conditions:

1. 2 h at − 15 °C; and
2. 2 h at + 15 °C and water immersion.

The weight loss was measured monthly (Table 5; each value is a result of three measurements).

Table 7
Weathering test

Sample	Mass loss (%)	Superficial aspect
A	0.4	No change
B	0.3	No change
C	0.2	Few yellowish spots
D	0.6	Few yellowish spots

Table 8
Sulphate attack

	A	B	C	D
Volume increases after 7 days (%)	3.8	16.7	2.8	3.7
Volume increases after 14 days (%)	4.3	70.8	5.8	4.7
Superficial aspect	No cracks are evident	Destruction of the specimen	Deep cracks are evident	Superficial cracks are evident

Table 9
Specific surface area measurements (BET, m^2/g)

Sample	7 days at 23 °C/ 50% RH	28 days at 23 °C/ 50% RH	After acid immersion
A	2.96	2.65	5.60
B	9.36	8.13	27.3
C	2.93	2.33	5.12
D	1.33	1.17	10.6

3.2.4. Taber abrasion test

The test simulates the mechanical abrasion to which a plaster is subjected during its service life. The experimental work was carried out by an instrument-type Taber model 30 according to the standard ISO 5470. Specimens ($100 \times 100 \times 10$ mm) were prepared and cured for 28 days. The weight loss was measured after 50 rotations of the rotating abrasive wheels (Table 6; the results are an average of three measurements).

3.2.5. Weathering test

The weathering test was carried out on render specimens ($40 \times 160 \times 10$ mm) after 28 days of curing. The samples were weathered for 1000 cycles in a weatherometer Atlas, model CI3000+, according to ASTM G26A (1 h and 40 min at 63 °C/50% RH, and 20 min at 50 °C and rain). The weight loss was determined and the superficial aspect was evaluated (Table 7).

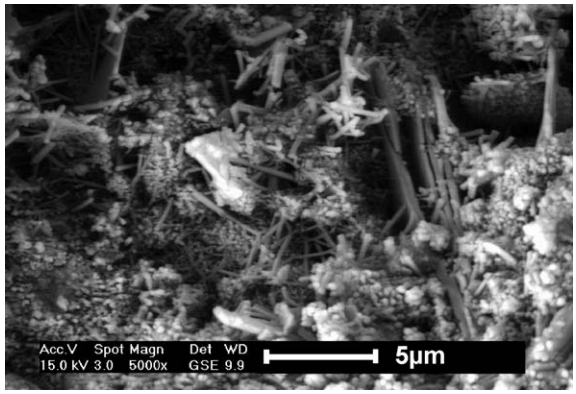

Fig. 4. SEM micrograph of Sample C after curing.

3.2.6. Sulphate attack

The experimental procedure to measure sulphate resistance (similar to Anstett's test [12]) was as follows:

1. Dry powder was sieved in order to separate large aggregates from fine materials.

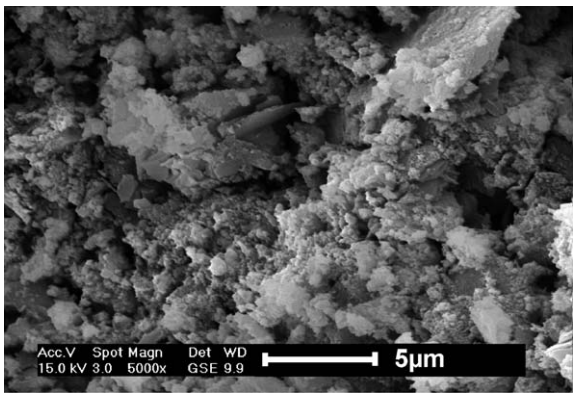

Fig. 2. SEM micrograph of Sample A after curing.

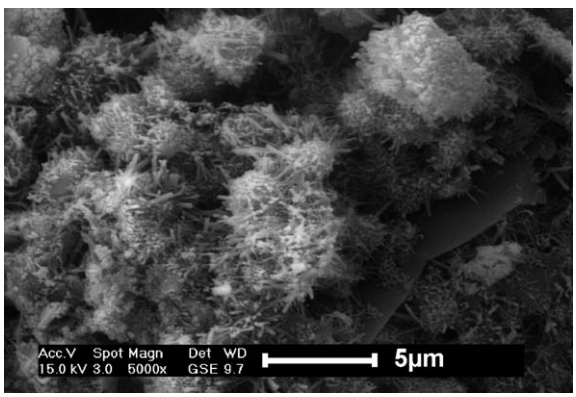

Fig. 3. SEM micrograph of Sample B after curing.

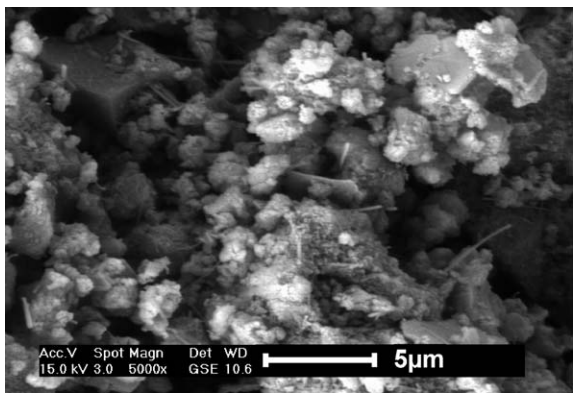

Fig. 5. SEM micrograph of Sample D after curing.

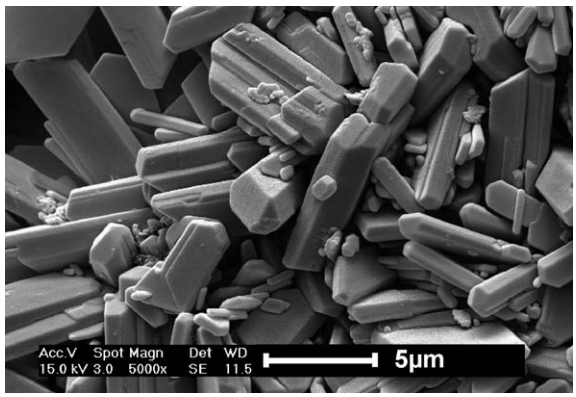

Fig. 6. SEM micrograph of Sample A at pH = 0.

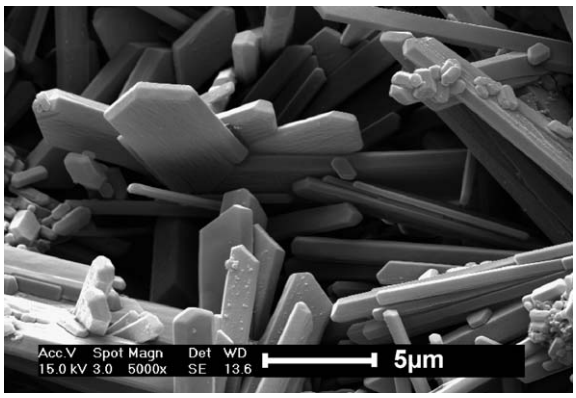

Fig. 7. SEM micrograph of Sample B at pH = 0.

2. Fine solid was mixed with 50% of water and cured for 28 days at 23 °C and 50% RH.
3. Hardened material was dried at 40 °C, ground, sieved (by a sieve having a light of 150 μm), and mixed with 50% gypsum and 6% water.
4. The mixture was moulded to obtain two cylindrical specimens (40 × 90 mm, height × diameter).

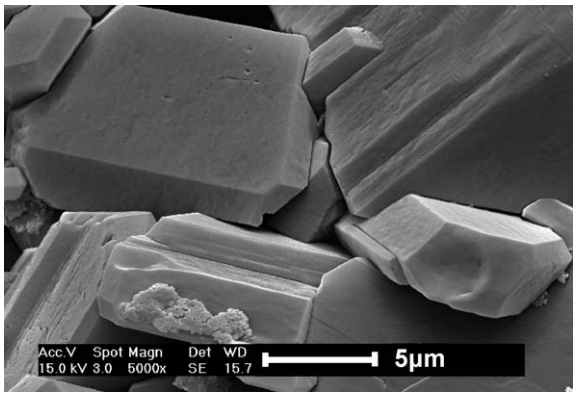

Fig. 8. SEM micrograph of Sample C at pH = 0.

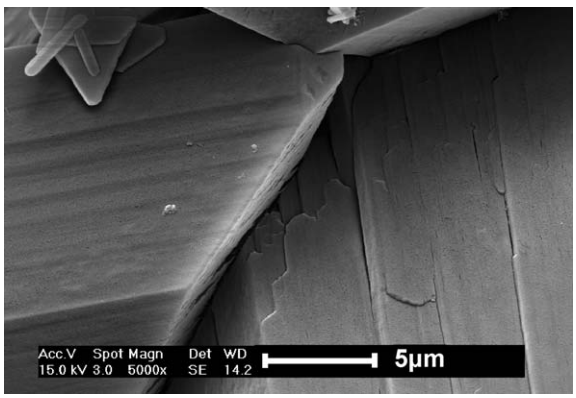

Fig. 9. SEM micrograph of Sample D at pH = 0.

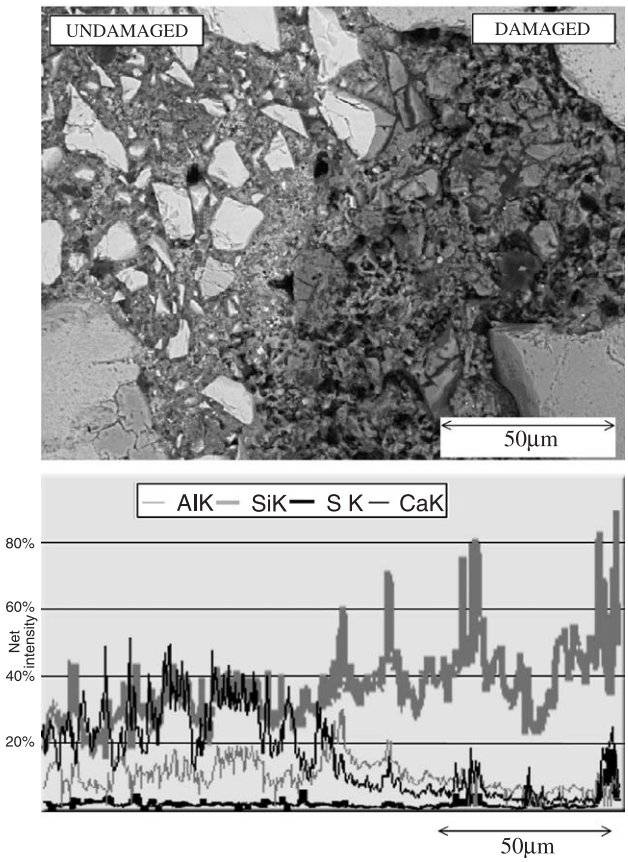

Fig. 10. EDS line scan of Specimen A.

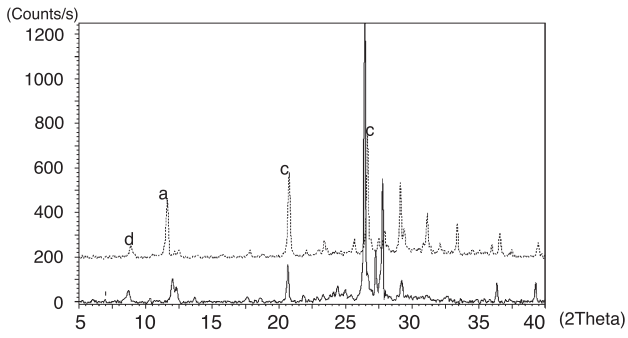

Fig. 11. XRD of Sample A (28 days of curing and after acid attack).

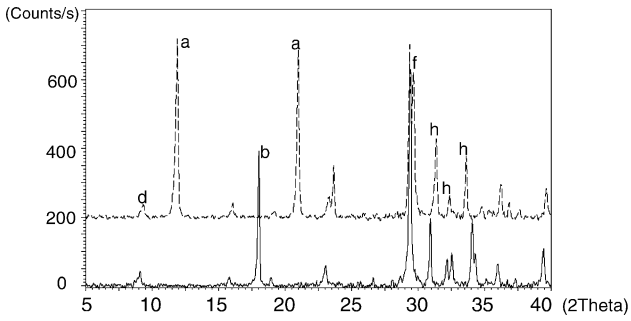

Fig. 12. XRD of Sample B (28 days of curing and after acid attack).

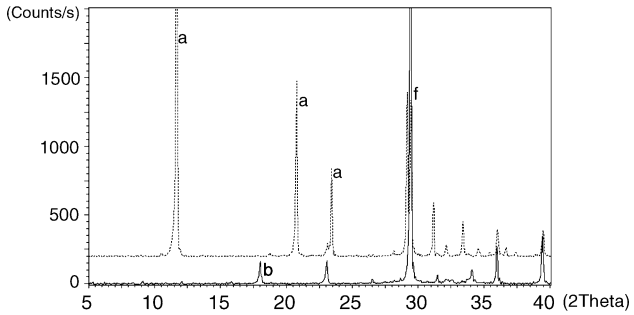

Fig. 13. XRD of Sample C (28 days of curing and after acid attack).

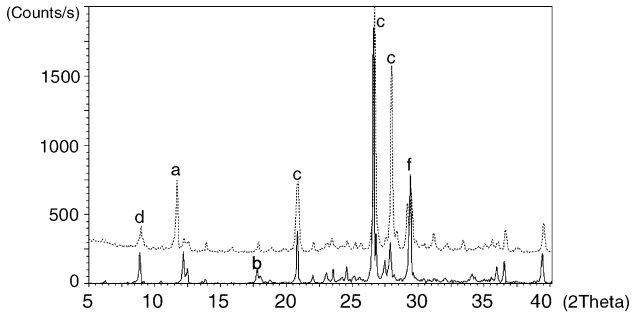

Fig. 14. XRD of Sample D (28 days of curing and after acid attack).

5. The samples were kept on a wetted tissue at 20 °C and 95% RH, and volume increase after 14 days was measured (Table 8).

3.3. Morphological and chemical analysis

The specific surface area (BET method) was measured on plaster specimens after 7 and 28 days of curing. Such analysis was carried out also on the samples subjected to sulphuric acid (Table 9).

Table 10
TG-DSC on the mortar samples

Sample	TG-DSC (%)				
	Phase	$t=28$ days	14 days pH = 0	Before sulphate attack	After sulphate attack
A	$Ca(OH)_2$	0.2	0.1	0.2	0.2
	$CaSO_4{\cdot}2H_2O$	2.8	13	34	65
B	$Ca(OH)_2$	5.2	0	3.3	2.8
	$CaSO_4{\cdot}2H_2O$	6.2	53	40	52.8
	$CaCO_3$	8.0	4.0	–	–
C	$Ca(OH)_2$	2.0	0.74	2	1.87
	$CaSO_4{\cdot}2H_2O$	0.4	39	35	46
	$CaCO_3$	83.6	49.2	–	–
D	$Ca(OH)_2$	0.9	0.45	1.1	0.7
	$CaSO_4{\cdot}2H_2O$	4.3	11.3	32	33.4
	$CaCO_3$	24	11	–	–

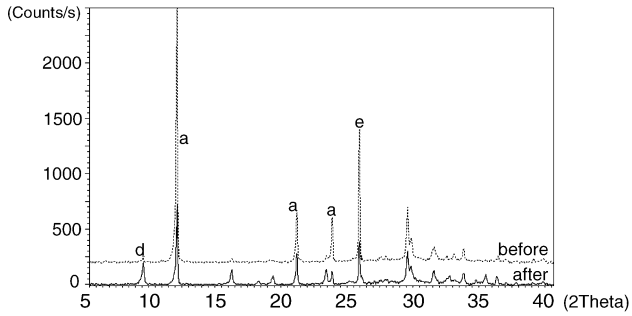

Fig. 15. XRD on Sample A before and after sulphate attack.

SEM analysis was performed on a fracture surface, which was covered with gold. In Figs. 2–5, SEM micrographs of plaster specimens after 28 days of curing at 23 °C and 50% RH are presented. In Figs. 6–9, SEM micrographs of mortars after sulphuric acid degradation are shown.

EDS line scan for SKα, CaKα, AlKα, and SiKα was carried out on polished sections of the specimens after acid attack. The study was focused on the border line between the unaltered region and the degraded one. An example of measurement is shown in Fig. 10.

XRD data were obtained using a Philips PW 1830 diffractometer with CuKα radiation. Thermogravimetric analysis and differential scanning calorimetry were executed by an apparatus-type Netzsch model STA409.

These analyses were performed on each sample after 28 days of curing (Figs. 11–14 and Table 10) and after

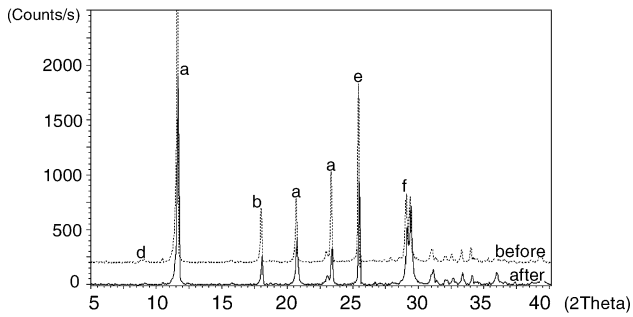

Fig. 16. XRD on Sample B before and after sulphate attack.

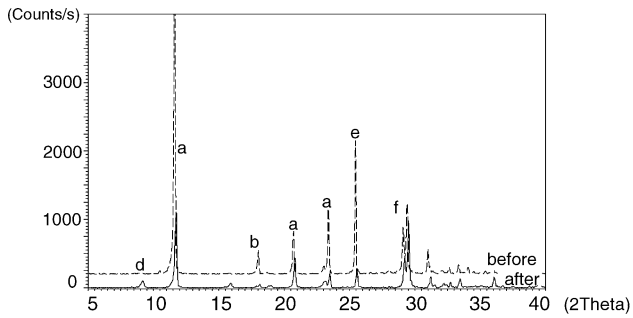

Fig. 17. XRD on Sample C before and after sulphate attack.

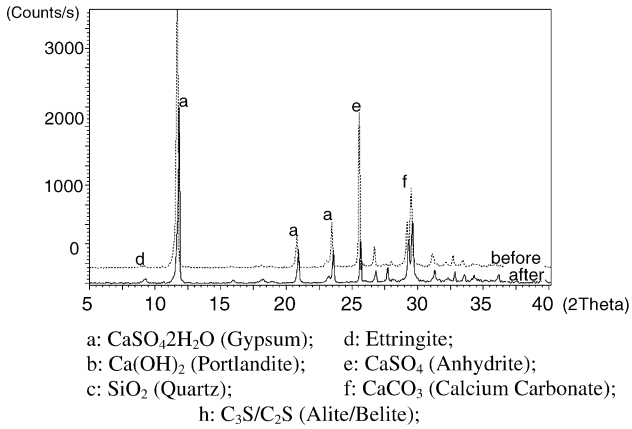

Fig. 18. XRD on Sample D before and after sulphate attack.

sulphuric acid (Figs. 11–14 and Table 10) and sulphate attack (Figs. 15–18 and Table 10).

4. Discussion

4.1. Mechanical properties

Rendering mortars are generally characterised by low mechanical performances as the material on which they are applied [6]. Obviously, a minimum requirement should be guaranteed to avoid mechanical damages. Slag mortar (A) is given the highest compressive strength (Table 2). The adhesion between plaster and masonry is another important property. Poor adhesion may be the cause of render detachment. Even in this case, Mortar A (Table 2) reached the best performances.

4.2. Physical properties

It is generally accepted that water is the medium through which plaster degradation occurs [5]. Therefore, water vapour permeability and water absorption are basic physical parameters to be considered for a correct plaster evaluation. In fact, high permeability allows a rapid water evaporation from the building materials, decreasing the moisture content. Water absorption could be related to the amount of polluting chemicals which can enter the plaster, causing damages. Air content (Table 2) is connected to fresh mortar porosity. In Table 2, the highest air content of Specimen C is evident. The hydraulic lime-based render had a low air content due to the absence of air-entraining admixture. The parameter-defined "total porosity" is associated with the amount of pores in the hardened material. A mortar porosity increase was detected with time (the effect is suggested by the higher total porosity with respect to initial air content and by the specific gravity decrease of the mortars after curing; Table 2). This behaviour is probably related to the water evaporation from rendering mortars. A direct relationship was found between air content and total porosity. The permeability to water vapour is expressed by the parameter μ, which is the moisture resistance factor. Samples B and C got the highest permeability to water vapour (the lowest μ value). The water absorption is directly connected to the total porosity (Table 2). In fact, Sample B (the highest total porosity) is characterised by a very high water absorption. The best system should be characterised by a compromise between water absorption (low) and permeability (high). Slag Mortar A satisfies these requirements.

4.3. Morphological analysis

A direct relationship was found between surface area (Table 9) and total porosity (Table 2).

For example, Sample B, which is characterised by the largest surface area, is the mortar with the highest total porosity. A specific surface area decrease was observed after curing. The effect is likely due to a possible hydrated lime carbonation [15]. Sulphuric acid reaction was emphasised by a large specific surface area increase connected to gypsum crystals precipitation. In Fig. 2, a SEM micrograph of Sample A (after 28 days of curing) is reported. A typical foil-like microstructure of hydrated slag was evident [13]. Portlandite was not visible. A SEM micrograph of Sample B is shown in Fig. 3. Fibrous gel-like material on spherical grains was evident. Furthermore, a porous network and hexagonal plates of calcium hydroxide with some rod-like needles were also visible. In Fig. 4 (Sample C), fibrillar material and some layers of calcium carbonate were emphasised. A SEM micrograph of Specimen D (Fig. 5) showed only a few regions of fibrous materials and some cubic crystals of aluminates. Acid attack causes a massive gypsum formation (Figs. 6–9). The surface of degraded samples is completely covered by gypsum. The largest gypsum crystals were detected in Fig. 9 (Specimen D). The effect is further confirmed by the highest specific surface area increase after acid attack (Table 9). Microcracks formation (Table 2) could favour crystals growth.

4.4. Chemical analysis

Hydration products of the mortars (Figs. 11–14 and Table 10), sulphuric acid, and sulphate attack (Figs. 15–18 and Table 10) were studied by XRD and TG-DSC. Concerning Specimen A, after 28 days of curing, only a very small amount of calcium hydroxide was noted (Fig. 11 and Table 10). Gypsum and ettringite were also detected. About Specimens B and C, a typical hydration pattern of Portland cement-based mortars was observed: portlandite formation and alite reduction (Figs. 12 and 13 and Table 10). Sample B (with a higher amount of Portland cement) is characterised by a larger amount of portlandite after 28 days of curing. Only a small amount of hydrated lime was detected (Fig. 14 and Table 10) for hydraulic lime-based render. C_2S (on which hydraulic lime is based) hydration causes a lower calcium hydroxide formation.

Sulphuric acid attack promotes a large gypsum precipitation. The expansive reaction connected with gypsum formation [10] is the main reason for render degradation. A decrease of calcium hydroxide and calcium carbonate (if present) was also evident. Ettringite development was not observed. This phase is not involved in the degradation process.

The data regarding sulphate attack are reported in Table 10 and Figs. 15–18. The degradation seems to be related to the reaction among calcium sulphate (in different hydrated forms), aluminates, and hydrated lime to give ettringite [2]. Gypsum, indicated in Table 10, is only an expression of water coming from sulphates expressed as $CaSO_4 \cdot 2H_2O$. The expansive effect related to ettringite precipitation causes swelling and cracks of the samples. Regarding EDS line scan, carried out on the specimens attacked by acid (an example is reported in Fig. 10), the following general trends were pointed out: an increase in the Ca/Si ratio in the unaltered region; presence of aluminium at the border line (in the case of Samples A and B); sulphur atoms (related to the gypsum phase) not detected in the first 100 μm between the border line and the degraded region (with the exception of Specimen D).

4.5. Durability

4.5.1. Physical durability test

The main causes of physical degradation of rendering mortars [5] are: (1) freezing and thawing cycles; (2) mechanical stress; and (3) weathering. The results, reported in Table 5, of freezing cycles pointed out a very good resistance of the slag-based render (A). Such kind of degradation is connected with stress arising from expansive ice formation in the pores. The better performances of Specimen A with respect to the other plasters could be due to a proper porosity distribution, lower water absorption, and higher mechanical performances.

The resistance to mechanical abrasion was evaluated by Taber abrasion test (Table 6). The parameter is related to mechanical properties, elasticity, and superficial smoothness of materials. Likely, Specimens A and B are given very good results for their mechanical resistance values.

Weathering test (Table 7) did not cause a substantial weight loss of the samples even if very critical conditions were used. Only small spots on Specimens C and D were noted. Such test results suggest that atmospheric factors (rain and sunshine) do not affect the integrity of the tested rendering mortars. Only a small alteration of the superficial aspect can occur.

4.5.2. Physical–chemical durability test

Three main aspects were analysed: (1) efflorescence, (2) acid attack, and (3) sulphate degradation. The data of the efflorescence test reported in Table 4 pointed out a good performance of Specimen A. In fact, only very small amounts of degraded material and salt were recovered on the plaster surface at the end of the mentioned cycle (Section 3.2.2). The slag-based rendering mortar is more resistant than the others renders to the degrading action of salt crystallisation. Furthermore, a small conductivity increase (connected to chloride concentration increase) was measured between 24 h and 28 days of cycles. This effect could be related to a lower capability of chlorides to pass through the specimen and a lower total porosity of the mortar. A direct connection was found between the conductivity increase and the amount of material recovered on the render surface.

The acid resistance of Samples A and B was very high (Table 3). The experimental results (Table 3) and the chemical analysis (Figs. 11–14 and Table 10) have shown the dependence of acid resistance on three main parameters: (1) high porosity, (2) low content of calcium hydroxide, and (3) absence of calcium carbonate. In fact, high porosity could balance the stress due to expansive gypsum formation (Sample B). A low concentration of calcium hydroxide allows a reduction of gypsum formation (Samples A and D in Table 10). A high amount of calcium carbonate is deleterious for the high reactivity of this salt with acidic substances (it is the cause of poor acidic resistance of Sample C; Table 3). The slag-based mortar is characterised by a proper combination of these three factors. Further information about the mechanism of acid attack was obtained from the EDS analysis (Fig. 10, Section 4.4). Considering the low Ca/Si ratio and the absence of gypsum in the first 100 μm between the border line and the degraded region, Ca ions could diffuse toward the region at lower pH (external region) where gypsum formation occurs. The progression of acid attack could be summarised in the following way:

1. The decrease of hydrated lime content near the border line causes pH lowering.
2. Other Ca ions can reach the regions from the inside part of the mortar, determining the progression of the border line inside the specimen.
3. Sulphate ions migrate, by diffusion, toward the internal part of the sample where they react with calcium to give gypsum.

Aluminium and iron silicate insoluble complexes formation at the border line during an acid attack was already observed by Chandra [16]. This effect could be due to a stabilisation of these complexes at the pH of the pore solution near the border line.

Specimens A and D (Table 8) showed the highest sulphate resistance. From XRD (Figs. 15–18) and TG-DSC measurements (Table 10), a relation was found between content of calcium hydroxide and mortar expansion. Furthermore, it seems that ettringite amount does not affect the expansion. These results are consistent with the existence of a colloidal and a crystalline ettringite. Colloidal ettringite (favoured by hydrated lime) is able to absorb water, causing a deleterious swelling [14]. In fact, in the case of slag-based render (A), due to a low amount of calcium hydroxide, crystalline ettringite is

formed (XRD after sulphate attack reported in Fig. 15). Therefore, the sample does not expand very much. Due to higher calcium hydroxide content, a high amount of colloidal ettringite is formed in the case of Specimen B (lower concentration of crystalline ettringite in the XRD). Also in this case, slag-based render reached good performances.

5. Conclusion

This study pointed out that the use of slag for rendering purposes is highly desirable, in particular under an ecological point of view. Furthermore, long plaster durability could be obtained if the product is properly optimised in order to have low water absorption, high permeability, low content of calcium hydroxide, and absence of calcium carbonate.

Acknowledgements

We are grateful for the precious collaboration of Mr. Cavagnini Andrea, Mrs. Maria Rosa Gulfo, and Mr. Dario Nicoletti of MAPEI SPA.

References

[1] M.T. Blanco-Varela, F. Puertas, A. Palomo, Rendering mortars in Medina Azahara: Part. I. Material characterization and alteration process, Mater. Constr. 47 (245) (1997) 29–43.
[2] M. Collepardi, Degradation and restoration of masonry walls of historical buildings, Mater. Struct. 23 (1990) 81–102.
[3] G. Moriconi, M. Castellano, M. Collepardi, Mortar deterioration of the masonry walls in historic buildings, a case history: Vanvitelli's mole in Ancona, Mater. Struct. (27) (1994) 408–414.
[4] N.P.H. Andrade, H. Carasen, F.N. Veiga, The use of SEM and XRD to diagnose problems in rendering mortar of buildings, Proceedings of 14th Congress of Electron Microscopy, Miguel Institute of Physics Publishing, Cancun, 1998, pp. 757–798.
[5] G.G. Amoroso, V. Fassina, Stone decay and conservation, Materials Science Monograph, vol. 11, Elsevier, Oxford, 1983, pp. 2–48.
[6] M. Collepardi, L. Coppola, in: L. ENCO (Ed.), Materiali Negli Edifici Storici: Degrado e Restauro, Enco Editor, Treviso, Italy, 1991.
[7] E. Blake, Ancient Roman Construction in Italy from the Prehistoric Period to Augustus, Carnegie Institution, Washington, DC, 1947.
[8] J. Pera, M. Chabannet, Durability of alkali-activated slag cements, in: K. Scrivener, J.F. Young (Eds.), Proceedings of the Materials Research Society Symposium, London, 1997, pp. 281–288.
[9] D.M. Roy, Hydration, microstructure, and chloride diffusion of slag cement pastes and mortars, American Concrete Institute, Fly Ash, Silica Fume, Slag, Natural Pozzolans and Concrete, vol. 2, American Concrete Institute, Trondheim, Norway, 1989, pp. 1265–1281.
[10] T. Cerulli, C. Pistolesi, C. Maltese, D. Salvioni, G. Facchetti, Durability of cement mortars to sulphuric acid attack, in: V.M. Malhotra (Ed.), CANMET/ACI on Durability of Concrete, Barcelona, 2000, pp. 357–371.
[11] I.S. Evans, Salt crystallization and rock weathering: a review, Rev. Geomorphol. Dyn. 4 (1970) 1–177.
[12] M. Collepardi, Il degrado chimico causato dal restauro delle murature degli edifici storici, L'Edilizia 10 (1989) 493–501.
[13] I.G. Richardson, G.W. Groves, Microstructure and microanalysis of hardened cement pastes involving ground granulated blast-furnace slag, J. Mater. Sci. 27 (1992) 6204–6212.
[14] P.K. Metha, Mechanism of expansion associates with ettringite formation, Cem. Concr. Res. 3 (1976) 1–6.
[15] J.J. Thomas, J. Hsieh, H.M. Jennings, Effect of carbonation on the nitrogen BET surface area of hardened Portland cement paste, Adv. Cem. Based Mater. 3 (1996) 76–80.
[16] S. Chandra, Hydrochloric acid attack on cement mortar—an analytical study, Cem. Concr. Res. 18 (1983) 193–203.